Journal of Science and Transport Technology
Journal homepage: https://jstt.vn/index.php/en

Article info
Type of article:
Original research paper

DOI:
https://doi.org/10.58845/jstt.utt.2026.en.6.1.143-160

***Corresponding author:**
Email address:
lientv@huce.edu.vn

Received: 30/01/2026
Received in Revised Form: 11/02/2026
Accepted: 09/03/2026

Free vibration of cracked multi-span continuous functionally graded nanobeams

Tran Binh Dinh, Tran Van Lien*
Hanoi University of Civil Engineering, 55 Giai Phong Street, Hanoi 100000, Vietnam

Abstract: The free vibration of multiple cracked multi-span continuous functionally graded (FG) nanobeams is investigated based on Eringen's nonlocal elastic theory (ENET). The massless three-spring model is employed to model transverse edged cracks. The governing equations for multiple cracked FG Euler–Bernoulli nanobeams are established by employing Hamilton's principle, the ENET, and conditions of continuity at the crack locations. Analytical solutions are obtained to construct the dynamic stiffness matrix of nanobeam element. The proposed matrix enables an efficient and highly accurate free vibration analysis of cracked FG multi-span nanobeams while requiring only a minimal number of elements. The accuracy of the present approach is verified through numerical validations with previous works. The influences of nonlocal, material, and geometric parameters on the free vibration of multiple-cracked multi-span FG nanobeams are investigated in detail.

Keywords: FG, Crack, ENET, DSM, Multi-span continuous nanobeam.

1. Introduction

An advanced class of composite materials, known as Functionally Graded Materials (FGMs), is designed to provide excellent thermal and mechanical properties, thereby improving the performance and reliability of structural components. FGMs are widely utilized in nanoscale applications such as nanobeams, nanotubes, and nanoplates within NEMS/MEMS devices. These applications encompass energy harvesters, fluid-conveying systems, nano-switches, nano-actuators, nano-sensors, nano-resonators, where high sensitivity and customized performance are crucial.

Classical elasticity theory fails to account for size-dependent effects at the micro/nanoscale, where structural dimensions become comparable to interatomic distances. To overcome this limitation, Eringen introduced the Nonlocal Elasticity Theory (ENET) in 1972. ENET assumes that the stress at a point is influenced by both the local strain and the strains at neighbouring points. Since its introduction, ENET has been extensively applied to investigate the mechanical behaviour of micro/nanostructures fabricated from homogeneous materials [1-4] and FGMs [5].

Crack initiation in micro/nanostructures may be attributed to atomic defects [6] or fabrication-induced thermal expansion [7]. Most existing studies on the free vibration of nanostructures have concentrated on intact FG nanostructures, while investigations involving cracked configurations are still limited. Among various crack modeling techniques, the elastic massless spring model is the most widely employed in the analysis of cracked nanobeams. Souq et al. [8] concluded that

empirical crack models formulated at the macroscale can be effectively and reliably employed in the vibration analysis of nanostructures.

Only a limited number of studies have addressed the bending, vibration and stability behaviour of cracked FG nanostructures within the framework of the ENET, including works by Soltanpour et al. [9], Ghadiri et al. [6], Esen et al. [10], and Attia et al. [11]. Except for Refs. [12, 13], all existing studies have focused on FG nanobeams subjected to simply supported ends or clamped ends containing a single crack. For a nanobeam containing n cracks, the natural frequencies and mode shapes are obtained by solving a 4(n+1)-order determinant that combines 4 boundary conditions with 4n continuity conditions at the crack locations, leading to a rapidly increasing computational effort as n increases. Lien et al. [14] derived analytical solutions for FG nanobeams containing n cracks under different boundary conditions, in which the natural frequencies and mode shapes are determined by solving only a 3rd-order determinant, regardless of the number of cracks.

Although ENET is widely applied in the study of micro/nanostructures, inconsistencies known as non-local paradoxes can arise in bending and vibration analyses of nanostructures [15-21]. Similar inaccuracies have been reported in many recent publications [11, 22]. The resolution of this issue has attracted significant research attention. Challamel et al. [23] introduced a discrete modelling approach, whereas an integro-differential alternative to the ENET was presented by Khodabakhshi and Reddy [24]. Furthermore, Aria and Friswell [25], along with Numanoglu and Civalek [26], employed finite element formulations based on the weighted residual method. Recently, Xu et al. [27] and Lien et al. [14, 28, 29] utilized the governing equations in their weak form to derive physically accurate and variational-consistent boundary conditions.

It has been observed that the FEM, as an approximate approach dependent on the choice of shape functions, may fail to accurately capture higher natural frequencies and corresponding mode shapes, even when refined meshes and higher-order elements are employed [30, 31]. The dynamic stiffness method (DSM) provides an excellent alternative to the FEM by overcoming its limitations. The DSM uses shape functions derived from exact analytical solutions, offering high accuracy for high-frequency responses. Its results are independent of mesh refinement and element selection, even with a minimal number of elements [32-35]. Adhikari et al. [1], [36], Taima et al. [37] applied the DSM to investigate the free vibration of FG nanobeams. More recently, Lien et al. [28, 29, 38, 39] proposed a nonlocal DSM for intact FG nanobeams by incorporating both Euler–Bernoulli beam and Timoshenko beam.

Despite existing studies on FG nanobeams, a comprehensive investigation of the free vibration of multiple cracked multi-span continuous FG nanobeams remains absent from the literature. In the present study, by using the DSM, the free vibration of multiple cracked multi-span continuous FG nanobeams is analysed. The dynamic stiffness matrix is constructed from analytical solutions of the motion equations for multiple cracked FG Euler–Bernoulli nanobeam elements. These solutions successfully eliminate the nonlocal paradox commonly observed in cantilever nanobeams. The reliability and accuracy of the proposed model are confirmed through comparisons with available published works. Furthermore, a comprehensive parametric study is performed to investigate the effects of material properties, geometric characteristics, crack configurations, and nonlocal parameters on the free vibration of multiple cracked multi-span continuous FG nanobeams.

2. Intact FG nanobeam element

In this paper, an FG nanobeam is considers with material properties that vary continuously through the thickness, given by [40]

$$E(z) = E_1 + (E_2 - E_1)(z/h + 0.5)^n$$
$$\rho(z) = \rho_1 + (\rho_2 - \rho_1)(z/h + 0.5)^n \quad (1)$$

where n is the volume fraction index; E and ρ denote elastic modulus and mass density, respectively; 2 and 1 denote respectively the top and bottom layers; z represents the thickness coordinate with its origin located at the mid-plane of the nanobeam (Fig. 1). The displacements of the Euler-Bernoulli nanobeam are represented as follows:

$$u(x,z,t) = u_0(x,t) - (z - h_0)\frac{\partial w(x,t)}{\partial x}$$
$$w(x,z,t) = w_0(x,t) \quad (2)$$

where $u_0(x,t)$ denotes the longitudinal displacement; the transverse deflection of the neutral plane is denoted by $w_0(x,t)$; h_0 represents the offset distance between the neutral axis and the x-axis [41]. The constitutive equations of the nanobeam based on ENET are expressed as [42]:

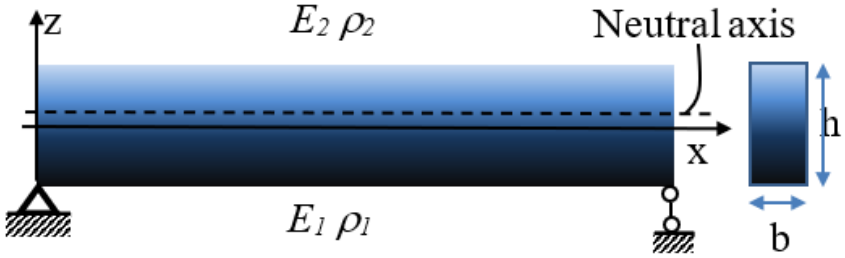

Fig. 1. An FG nanobeam

$$\sigma_{xx} - \mu\frac{\partial^2\sigma_{xx}}{\partial x^2} = E\varepsilon_{xx} \quad (3)$$

where μ is the nonlocal parameter. Let A_{11}, A_{12}, and A_{22} denote the rigidities, and I_{11}, I_{12}, and I_{22} denote the mass moments, respectively

$$A_{11} = \int_A E(z)dA;\ A_{12} = \int_A (z - h_0)E(z)dA$$
$$A_{22} = \int_A (z - h_0)^2 E(z)dA;\ I_{11} = \int_A \rho(z)dA \quad (4)$$
$$I_{12} = \int_A (z - h_0)\rho(z)dA;\ I_{22} = \int_A (z - h_0)^2\rho(z)dA$$

Using Hamilton's principle, the equations of motion are expressed as [29]:

Eq. (5)

and the corresponding natural boundary conditions

Eq. (6)

It should be emphasized that Eq. (5), along with Eq. (6), do not satisfy the self-adjointness condition for nanostructures with free ends. To eliminate the paradoxical results, the weak form of Eq. (5) is established by weighting Eq. (5) with the virtual displacements δu_0 and δw_0, respectively, followed by integration over the beam length. Thence, the resulting variationally consistent boundary conditions are expressed as follows:

Eq. (7)

Eq. (7) presents the complete set of classical boundary conditions for the Euler–Bernoulli nanobeam. These boundary conditions satisfy the self-adjointness condition and coincide with those in Eq. (6) for clamped, simply supported and clamped–simply supported ends.

$$A_{11}\frac{\partial^2 u_0}{\partial x^2} - A_{12}\frac{\partial^3 w_0}{\partial x^3} + \mu\left(I_{11}\frac{\partial^4 u_0}{\partial x^2\partial t^2} - I_{12}\frac{\partial^5 w_0}{\partial x^3\partial t^2}\right) - I_{11}\frac{\partial^2 u_0}{\partial t^2} + I_{12}\frac{\partial^3 w_0}{\partial x\partial t^2} = 0$$
$$A_{12}\frac{\partial^3 u_0}{\partial x^3} - A_{22}\frac{\partial^4 w_0}{\partial x^4} + \mu\left[I_{11}\frac{\partial^4 w_0}{\partial x^2\partial t^2}\ddot{w}_{0,xx} + I_{12}\frac{\partial^5 u_0}{\partial x^3\partial t^2}\ddot{u}_{0,xxx} - I_{22}\frac{\partial^6 w_0}{\partial x^4\partial t^2}\right] - I_{11}\frac{\partial^2 w_0}{\partial t^2} - I_{12}\frac{\partial^3 u_0}{\partial x\partial t^2} + I_{22}\frac{\partial^4 w_0}{\partial x^2\partial t^2} = 0 \quad (5)$$

$$N = A_{11}\frac{\partial u_0}{\partial x} - A_{12}\frac{\partial^2 w_0}{\partial x^2} + \mu\left(I_{11}\frac{\partial^3 u_0}{\partial x\partial t^2} - I_{12}\frac{\partial^4 w_0}{\partial x^2\partial t^2}\right)$$
$$M = A_{12}\frac{\partial u_0}{\partial x} - A_{22}\frac{\partial^2 w_0}{\partial x^2} + \mu\left(I_{12}\frac{\partial^3 u_0}{\partial x\partial t^2} + I_{11}\frac{\partial^2 w_0}{\partial t^2} - I_{22}\frac{\partial^4 w_0}{\partial x^2\partial t^2}\right) \quad (6)$$

$$Q = A_{12}\frac{\partial^2 u_0}{\partial x^2} - A_{22}\frac{\partial^3 w_0}{\partial x^3} - I_{12}\frac{\partial^2 u_0}{\partial t^2} + I_{22}\frac{\partial^3 w_0}{\partial x \partial t^2} + \mu\left(I_{12}\frac{\partial^4 u_0}{\partial x^2 \partial t^2} + I_{11}\frac{\partial^3 w_0}{\partial x \partial t^2} - I_{22}\frac{\partial^5 w_0}{\partial x^3 \partial t^2}\right)$$

$$N = A_{11}\frac{\partial u_0}{\partial x} - A_{12}\frac{\partial^2 w_0}{\partial x^2} + \mu\left(I_{11}\frac{\partial^3 u_0}{\partial x \partial t^2} - I_{12}\frac{\partial^4 w_0}{\partial x^2 \partial t^2}\right)$$

$$M = A_{22}\frac{\partial^2 w_0}{\partial x^2} \tag{7}$$

$$Q = A_{12}\frac{\partial^2 u_0}{\partial x^2} - A_{22}\frac{\partial^3 w_0}{\partial x^3} + I_{22}\frac{\partial^3 w_0}{\partial x \partial t^2} + \mu\left(I_{12}\frac{\partial^4 u_0}{\partial x^2 \partial t^2} + I_{11}\frac{\partial^3 w_0}{\partial x \partial t^2} - I_{22}\frac{\partial^5 w_0}{\partial x^3 \partial t^2}\ddot{w}_{0,xxx}\right)$$

By applying the Fourier transform, Eq. (5) and (7) are transformed into the frequency domain as follows:

Eq. (8)

and

Eq. (9)

where

Eq. (10)

By assuming the solutions of Eq. (8) in the following form $\{\mathbf{z}_0\} = e^{\lambda x}\{\mathbf{d}\}$, one obtains:

Eq. (11)

Non-zero solutions of Eq. (11) exist when the determinant vanishes. Expanding the resulting characteristic equation leads to a cubic polynomial in $\eta=\lambda^2$:

Eq. (12)

where

Eq. (13)

Let the solutions of the cubic Eq. (12) be denoted as η_1, η_2, η_3 and:

Eq. (14)

Eq. (15)

Thence, the solutions of Eq. (8) are expressed as follows:

Eq. (16)

where $[\mathbf{G}_0(x,\omega)]$ is the matrix

Eq. (17)

$$[\mathbf{A}_4]\frac{d^4\{\mathbf{z}\}}{dx^4} + [\mathbf{A}_3]\frac{d^3\{\mathbf{z}\}}{dx^3} + [\mathbf{A}_2]\frac{d^2\{\mathbf{z}\}}{dx^2} + [\mathbf{A}_1]\frac{d\{\mathbf{z}\}}{dx} + [A_0]\{\mathbf{z}\} = \{0\} \tag{8}$$

$$(N\,M\,Q)^T = [b_F]\{z\} \tag{9}$$

$$\{z\} = \begin{pmatrix} U(x,\omega) \\ W(x,\omega) \end{pmatrix} = \int_{-\infty}^{\infty}\begin{pmatrix} u_0(x,t) \\ w_0(x,t) \end{pmatrix} e^{-i\omega t}dt$$

$$[A_4] = \begin{pmatrix} 0 & 0 \\ 0 & A_{22} - \mu I_{22}\omega^2 \end{pmatrix}$$

$$[A_3] = \begin{pmatrix} 0 & -\left(A_{12} - \mu I_{12}\omega^2\right) \\ -\left(A_{12} - \mu I_{12}\omega^2\right) & 0 \end{pmatrix}$$

$$[A_2] = \begin{pmatrix} 0 & -I_{12}\omega^2 \\ -I_{12}\omega^2 & 0 \end{pmatrix} \tag{10}$$

$$[A_1] = \begin{pmatrix} A_{11} - \mu I_{11}\omega^2 & 0 \\ 0 & I_{22}\omega^2 + \mu I_{11}\omega^2 \end{pmatrix}$$

$$[A_0] = \begin{pmatrix} I_{11}\omega^2 & 0 \\ 0 & -I_{11}\omega^2 \end{pmatrix}$$

$$[b_F]=\begin{bmatrix}\left[A_{11}-\mu I_{11}\omega^2\right]\partial_x & -\left(A_{12}-\mu I_{12}\omega^2\right)\partial_x^2\\ 0 & A_{22}\partial_x^2\\ \left(A_{12}-\mu I_{12}\omega^2\right)\partial_x^2 & \left[-\left(I_{22}+\mu I_{11}\right)\omega^2\right]\partial_x-\left(A_{22}-\mu I_{22}\omega^2\right)\partial_x^3\end{bmatrix}$$

$$\left(\lambda^4[\mathbf{A}_4]+\lambda^3[\mathbf{A}_3]+\lambda^2[\mathbf{A}_2]+\lambda[\mathbf{A}_2]+[A_1]\right)\{\mathbf{d}\}=\{0\} \quad (11)$$

$$a\eta^3+b\eta^2+c\eta+d=0 \quad (12)$$

$$a=\mu^2\left(I_{11}I_{22}-I_{12}^2\right)\omega^4-\mu\left(A_{11}I_{22}-2A_{12}I_{12}+A_{22}I_{11}\right)\omega^2+A_{11}A_{22}-A_{12}^2$$

$$b=-\mu\left[2\left(I_{11}I_{22}-I_{12}^2\right)+\mu I_{11}^2\right]\omega^4+\left(\begin{matrix}\mu I_{11}A_{11}+A_{11}I_{22}-\\ -2A_{12}I_{12}+A_{22}I_{11}\end{matrix}\right)\omega^2 \quad (13)$$

$$c=\left(I_{11}I_{22}-I_{12}^2+2\mu I_{11}^2\right)\omega^4-A_{11}\omega^2$$

$$d=-I_{11}^2\omega^4$$

$$\lambda_{1,4}=\pm\sqrt{\eta_1};\lambda_{2,5}=\pm\sqrt{\eta_2};\lambda_{3,6}=\pm\sqrt{\eta_3} \quad (14)$$

$$\alpha_j=k_j\frac{\left(A_{12}-\mu I_{12}\omega^2\right)k_j^2+I_{12}\omega^2}{\left(A_{11}-\mu I_{11}\omega^2\right)k_j^2+I_{11}\omega^2};j=\overline{1,3} \quad (15)$$

$$\{Z_0(x)\}=\{U,W,W',W''\}^T=[\mathbf{G}_0(x)]\{\mathbf{C}\} \quad (16)$$

$$\left[G_0(x)\right]=\begin{pmatrix}\alpha_1e^{k_1x} & \alpha_2e^{k_2x} & \alpha_3e^{k_3x} & -\alpha_1e^{-k_1x} & -\alpha_2e^{-k_2x} & -\alpha_3e^{-k_3x}\\ e^{k_1x} & e^{k_2x} & e^{k_3x} & e^{-k_1x} & e^{-k_2x} & e^{-k_3x}\\ k_1e^{k_1x} & k_2e^{k_2x} & k_3e^{k_3x} & -k_1e^{-k_1x} & -k_2e^{-k_2x} & -k_3e^{-k_3x}\\ k_1^2e^{k_1x} & k_2^2e^{k_2x} & k_3^2e^{k_3x} & k_1^2e^{-k_1x} & k_2^2e^{-k_2x} & k_3^2e^{-k_3x}\end{pmatrix} \quad (17)$$

3. Cracked FG nanobeam element

A transverse edged crack located at z=ze in the FG nanobeam is represented by three massless elastic springs that connect the intact segments (Fig. 2). The continuity conditions at the cracked cross-section are expressed as [43]

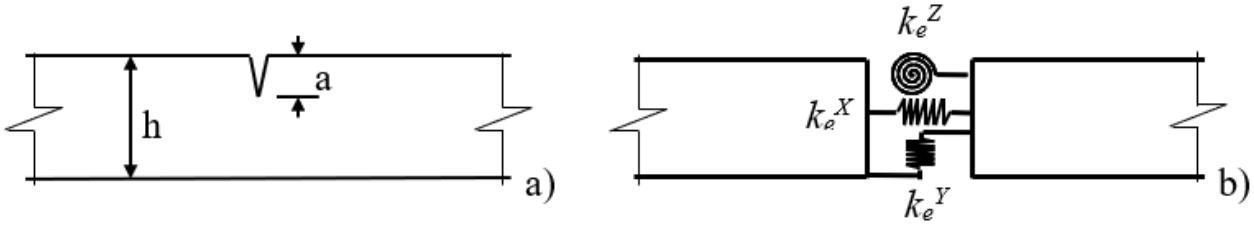

Fig. 2. A transverse edged crack and equivalent massless three-springs model

$$\begin{aligned}&U(z_e+0)=\gamma_1.U'(z_e)+U(z_e-0)\\ &W(z_e+0)=-\gamma_3.W'''(z_e)+W(z_e-0)\\ &W'(z_e+0)=-\gamma_2.W''(z_e)+W'(z_e-0)\\ &U'(z_e+0)=U'(z_e-0)\\ &W''(z_e+0)=W''(z_e-0)\\ &W'''(z_e+0)=W'''(z_e-0)\end{aligned} \quad (18)$$

where

$$\gamma_1=\frac{A_{11}}{k_e^X};\gamma_2=\frac{A_{22}}{k_e^Z};\gamma_3=\frac{A_{22}}{k_e^Y} \quad (19)$$

The parameters γ_1, γ_2, and γ_3 are functions of the material, geometric and crack properties of the FG nanobeam. These parameters are taken to be equivalent to those of an associated homogeneous nanobeam. Thence, these parameters are evaluated as follows:

$$\begin{aligned}&\gamma_1=2\pi(1-\nu^2)h\phi_1f_1(\xi);\\ &\gamma_2=6\pi(1-\nu^2)h\phi_2f_2(\xi);\\ &\gamma_3=2\pi(1-\nu^2)h^3\phi_2f_3(\xi)\end{aligned} \quad (20)$$

where ξ=a/h; ϕ_1 and ϕ_2 are functions of FG parameters [43]:

$$\phi_1 = \frac{2(R_e + n)}{(R_e + 1)(1+n)}; R_e = \frac{E_t}{E_b}; \alpha = 0.5 + \frac{h_0}{h}$$
$$\phi_2 = \frac{24}{R_e + 1}\left[\frac{3R_e + n}{3(3+n)} - \frac{2R_e + n}{2+n}\alpha + \frac{R_e + n}{1+n}\alpha^2\right] \quad (21)$$

f_1, f_2, and f_3 are functions obtained from mechanics of fractures [44-46]:

Eq. (22)

The solution of Eq. (11) that satisfies Eq. (18) at the crack is expressed as:

Eq. (23)

where $[\mathbf{G}_C(x)]$ is a particular solution; $\{Z_0'(z_e)\}$ is the vector:

Eq. (24)

The analytical solution of Eq. (11) is obtained through the principle of the superposition as follows:

Eq. (25)

Applying the recurrence theorem, the matrix $\bar{\Psi}$ is expressed as:

Eq. (26)

where $\left[\bar{X}_j\right]$ is:

Eq. (27)

$$f_1(\xi) = 0.6272\xi^2 - 0.17248\xi^3 + 5.92134\xi^4 - 10.7054\xi^5 + 31.5685\xi^6 - 67.47\xi^7 + 139.123\xi^8 - 146.682\xi^9 + 92.3552\xi^{10}$$
$$f_2(\xi) = 0.6272\xi^2 - 1.04533\xi^3 + 4.5948\xi^4 - 9.9736\xi^5 + 20.2948\xi^6 - 33.0351\xi^7 + 47.1063\xi^8 - 40.7556\xi^9 + 19.6\xi^{10} \quad (22)$$
$$f_3(\xi) = -2.1668\log(1-\xi) - 2.1668\xi - 1.0834\xi^2 + 0.6018\xi^3 + 4.9485\xi^4 + 0.4461\xi^5 - 10.9659\xi^6 + 9.3162\xi^7 - 2.5110\xi^8$$

$$\{Z_e(x)\} = [G_C(x)]\{Z_0'(z_e)\} \quad (23)$$

$$\{Z_0'(z_e)\} = \left(U_0'(z_e)\ W_0'(z_e)\ W_0''(z_e)\ W_0'''(z_e)\right)^T \quad (24)$$

$$\{Z_c(x)\} = \left(\left[\mathbf{G}_0(x)\right] + \left[\bar{G}_C(x - z_e)\right].\left[G_0'(z_e)\right]\right).\{C\} = [\bar{\Psi}(x)]\{C\} \quad (25)$$

$$\left[\bar{\Psi}(x)\right] = \left[G_0(x)\right] + \sum_{j=1}^{n}\left[\bar{G}_C(x - z_{e_j})\right].\left[\bar{X}_j\right] \quad (26)$$

$$\left[\bar{X}_j\right] = \left[G_0'(z_{e_j})\right] + \sum_{k=1}^{j-1}\left[\bar{G}_C'(z_{e_j} - z_{e_k})\right].\left[\bar{X}_k\right] \qquad j = \overline{1,n} \quad (27)$$

4. Dynamic stiffness matrix

For the FG nanobeam, the nodal displacement vector $\{\mathbf{U_e}\}$ and the corresponding nodal force vector $\{\mathbf{P_e}\}$ are determined as follows (Fig. 3):

$$\{\mathbf{U}_e\} = \{U_1, \Phi_1, W_1, U_2, \Phi_2, W_2\}^T$$
$$\{\mathbf{P}_e\} = \{N_1, M_1, Q_1, N_2, M_2, Q_2\}^T \quad (28)$$

where

$$U_1 = U(0);\ U_2 = U(L)$$
$$\Phi_1 = W'(0);\ \Phi_2 = W'(L)$$
$$W_1 = W(0);\ W_2 = W(L) \quad (29)$$
$$(N_1\ M_1\ Q_1) = -\left[B_F\right](U\ W\ W'\ W'')\big|_{x=0}$$
$$(N_2\ M_2\ Q_2) = \left[B_F\right](U\ W\ W'\ W'')\big|_{x=L}$$

and $\mathbf{B_F}$ is the boundary condition operator in Eq. (9) extended to the solution expression (24)

$$\left[\mathbf{B}_F\right] = \begin{bmatrix} \left(A_{11} - \mu I_{11}\omega^2\right)\partial_x & 0 & 0 & -\left(A_{12} - \mu I_{12}\omega^2\right) \\ 0 & 0 & 0 & A_{22} \\ \left(A_{12} - \mu I_{12}\omega^2\right)\partial_x^2 & 0 & -\left(I_{22} + \mu I_{11}\right)\omega^2 & -\left(A_{22} - \mu I_{22}\omega^2\right)\partial_x \end{bmatrix} \quad (30)$$

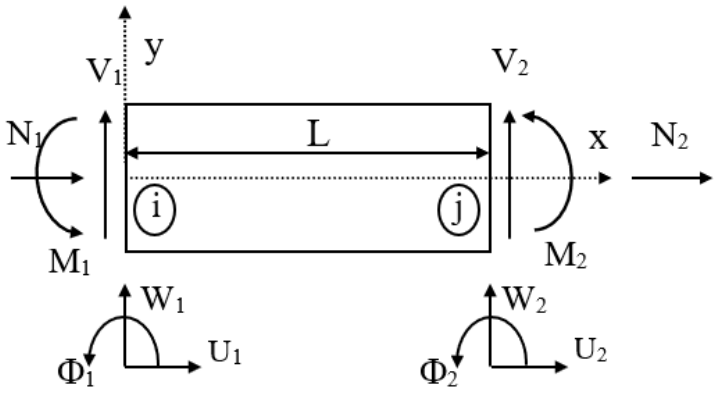

Fig. 3. A nanobeam element

Substitution of Eq. (26) into Eq. (29), followed by elimination of the vector $\{C\}$ yields:

$$\left[\bar{\mathbf{K}}_e(\omega)\right].\{\mathbf{U}_e\} = \{\mathbf{P}_e(\omega)\} \quad (31)$$

where the dynamic stiffness matrix is denoted by $\left[\bar{K}_e\right]$ for the cracked FG nanobeam, presented as

$$[\bar{\mathbf{K}}_e] = \begin{bmatrix} \left[-B_F\left(\bar{\Psi}\right)_{x=0}\right] \\ \left[B_F\left(\bar{\Psi}\right)_{x=L}\right] \end{bmatrix} . \begin{bmatrix} \left[\bar{\Psi}(0)\right] \\ \left[\bar{\Psi}(L)\right] \end{bmatrix}^{-1} \quad (32)$$

For the entire structure, by enforcing internal force equilibrium at each nodal point, the global stiffness matrix [**K**] is constructed. Denoting **U** as the global degree-of-freedom vector of the nanostructure, the equation of free vibrations is expressed as:

$$[\mathbf{K}].\{\mathbf{U}\} = \{0\} \quad (33)$$

Thence, natural frequencies can be obtained by setting the determinant of the matrix [**K**] to zero:

$$\det[\mathbf{K}] = 0 \quad (34)$$

The mode shape associated with the frequency ω_j is obtained as follows:

$$\{\varphi_j(x)\} = C_j^0\left[\bar{\mathbf{\Psi}}(x,\omega_j)\right].\begin{bmatrix} \left[\bar{\Psi}(0,\omega_j)\right] \\ \left[\bar{\Psi}(L,\omega_j)\right] \end{bmatrix}^{-1} \{U_j\} \quad (35)$$

where C_j^0 denote a constant, $\{\mathbf{U}_j\}$ represents the normalized eigenvector obtained from Eq. (33) associated with the natural frequency ω_j.

To determine the natural frequencies and corresponding mode shapes, a program in Matlab was established based on the Wittrick-William theorem [34], together with the Newton-Raphson method. The mode shape associated with the frequency ω_j is obtained by applying the SVD algorithm to Eq. (33) and Eq. (35).

5. Result and discussion

5.1. Validation

Table 1. The first nondimensional frequencies of the clamped-free FGM nanobeams

μ^*	n=0		n=0.2		n=1		n=10		n=∞	
	Present	[25]	Present	[25]	Present	[25]	Present	[25]	Present	[25]
0	1.0149	1.0149	1.2791	1.2791	1.5036	1.5036	1.8035	1.8035	1.9533	1.9533
1	1.0147	1.0147	1.2788	1.2788	1.5033	1.5033	1.8031	1.8031	1.9528	1.9528
2	1.0144	1.0144	1.2785	1.2785	1.5029	1.5029	1.8027	1.8027	1.9523	1.9523
3	1.0142	1.0142	1.2782	1.2782	1.5026	1.5026	1.8022	1.8022	1.9519	1.9519
4	1.0140	1.0140	1.2779	1.2779	1.5022	1.5022	1.8018	1.8018	1.9514	1.9514
5	1.0137	1.0137	1.2776	1.2776	1.5019	1.5019	1.8014	1.8014	1.9510	1.9510

The nondimensional forms of the nonlocal parameter and natural frequencies are introduced for convenience, as follows

$$\mu^* = \left(\frac{e_0 a}{h}\right)^2 ; \lambda_i = \frac{\omega_i L^2}{h}\sqrt{\frac{12\rho_m}{E_m}} \quad (36)$$

Table 1 demonstrates the excellent agreement between the first nondimensional frequencies of intact FG nanocantilevers computed by the proposed single-element DSM and those of Aria and Friswell [25], using 26 elements. For other boundary conditions, including simply supported ends, clamped–simply supported ends, and clamped-clamped ends, similar accuracy is achieved for the first natural frequency. Furthermore, the proposed formulation effectively resolves the nonlocal paradox typically encountered in cantilever nanobeams.

Table 2 demonstrates splendid agreement between the nondimensional first frequency ratios of cracked and intact homogeneous beams obtained in the present study and those reported by Aydin [47]. The numerical results validate the accuracy and reliability of the proposed model.

Table 2. The first frequency ratios of the homogeneous beam with a single crack

Cantilever	**x_1/L=0.2**	**x_1/L=0.4**	**x_1/L=0.6**
Aydin [47]	0.9906	0.9958	0.9982
Present	0.9928	0.9961	0.9984
Clamped-Clamped	**x_1/L=0.1**	**x_1/L=0.3**	**x_1/L=0.4**
Aydin [47]	0.9971	0.9963	0.9943
Present	0.9970	0.9960	0.9940
Simple-Simple	**x_1/L=0.2**	**x_1/L=0.4**	**x_1/L=0.7**
Aydin [47]	0.9959	0.9916	0.9985
Present	0.9968	0.9933	0.9991

5.2. Case study

The free vibration behaviour of multiple cracked multi-span continuous FG nanobeams is studied in this subsection (Fig. 4). The material properties are taken as: E_1=70 GPa, ρ_1=2700 kg/m^3, ν_1=0.3 for metal phases, and: E_2=393 GPa, ρ_2=3960 kg/m^3, ν_2=0.3 for ceramic phases [41]. The nanobeam was discretized into three elements connected at the supports, based on the previously specified geometric dimensions, namely the length and width.

Fig. 5 presents the change of first seven frequencies of the intact (solid lines) and multiple cracked multi-span continuous FG nanobeams with various nonlocal parameters: μ^*=0, 2, 4, 6. In this case, all beams contain either one crack at 2h from the left node (dashed lines) or two cracks at 2h and 4h (dotted lines), with the depth-to-height ratio of 0.2 for each crack (a/h=20%). It is observed that the presence of cracks and the increase in the nonlocal parameter both lead to a decrease in the nondimensional frequencies. Furthermore, the nonlocal parameter induces greater decreases in nondimensional frequencies than multiple cracks, especially in the higher-order modes.

The changes in the first three frequencies of the intact (solid lines) and cracked (dash lines) multi-span continuous FG nanobeam are presented in Fig. 6, with various nonlocal parameters: $\mu^* = 0,2,4,6$ and ratios: $1 \le E_2/E_1 \le 20$. All beams contain a single crack located at 2.5h from the left node with the ratio a/h=20%. A pronounced reduction in the natural frequencies is observed with increasing nonlocal parameter values, with the effect being amplified at higher modulus ratios E_2/E_1. The results reveal that higher-order modes are more sensitive to frequency reduction than lower-order modes. On the contrary, lower-order modes are more sensitive to crack-induced frequency reductions than higher-order modes.

The different first three frequencies of the intact (solid line) and the cracked (dash line) multi-span continuous FG nanobeam are presented in Fig. 7, with volume fraction indexes: $0 \le n \le 10$ and various nonlocal parameters: $\mu^* = 0,2,4,6$. All

beams contain a single crack located at 2.5h from the left node with the ratio a/h=20%. The results show that increasing values of the nonlocal parameter lead to a remarkable decrease in the natural frequencies, especially when the volume fraction index exceeds 1. Conversely, in the case of a volume fraction index less than 1, a remarkable increase in the natural frequencies is observed. Moreover, higher-order nondimensional natural frequencies experience a greater reduction compared with lower-order frequencies. On the contrary, the decrease in lower-order natural frequencies caused by cracks is greater than that obtained in higher-order frequencies.

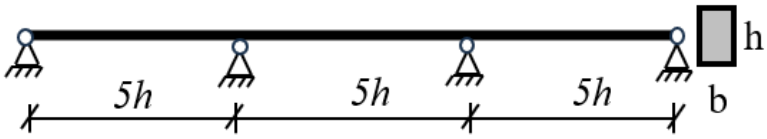

Fig. 4. A multi-span continuous nanobeam

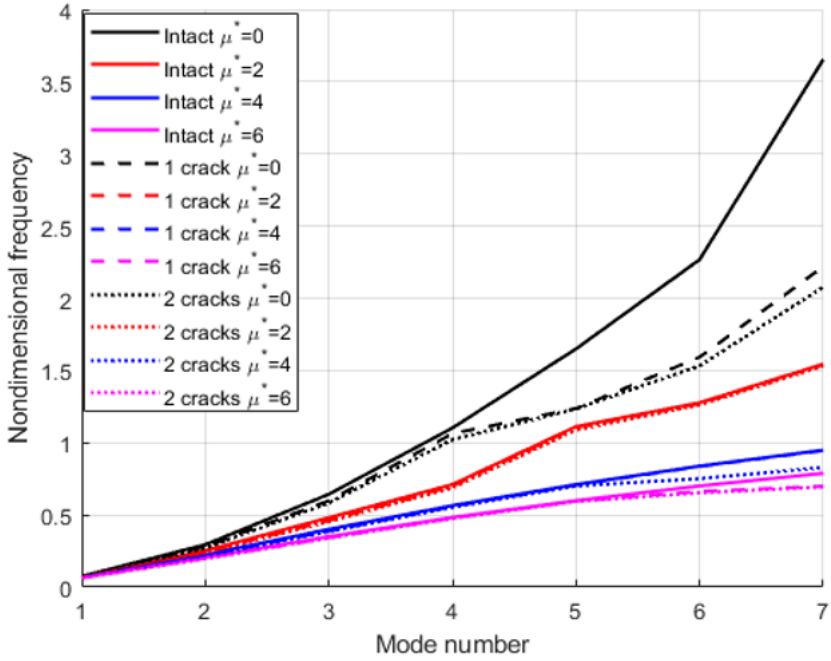

Fig. 5. Changes of first seven frequencies of the intact and the multiple cracked multi-span continuous FG nanobeam under nonlocal parameters: μ^*=0, 2, 4, 6.

Fig. 8 illustrates the variations of the first three frequency ratios of a multi-span continuous FG nanobeam with a single crack relative to the intact beam as the crack position varies along the beam length for: a/h=10%, a/h=20%, and a/h=30% at μ^*=2. When the ratio of crack depth-to-height increases and the crack is positioned at the mid-span, a remarkable decrease in the natural frequencies is observed. Lower-order frequencies exhibit a more significant reduction compared with higher-order ones. It is concluded that the lower-order frequencies exhibit greater sensitivity to the presence of cracks. Furthermore, the critical points at which a given natural frequency remains unaffected by cracks are not influenced by the nonlocal parameter. The identified critical points agree well with those reported for homogeneous and FG macro-scale beams. The critical point locations are independent of the number of cracks. Such information is highly beneficial for crack identification, as it identifies frequencies that are insensitive to crack presence.

The changes in the first three mode shapes and their corresponding deviations from the intact multi-span continuous FG nanobeam are illustrated in Fig. 9. Cracks with the same depth-to-height ratio of 20% are located at x=2h and 3h in the first and third span, and at x=2h and 4h in the

second span. Different scenarios are illustrated in these subfigures: (a) Mode shapes for μ^*=0, 2, and 4 (Fig. 9a); (b) Deviations of mode shapes for μ^*=0, 2, and 4 (Fig. 9b); (c) Mode shapes for E_2/E_1=0.1, 2, and 10 (Fig. 9c); (d) Deviations of mode shapes for E_2/E_1=0.1, 2, and 10 (Fig. 9d); (e) Mode shapes for n=0, 2, and 10 (Fig. 9e); (f) Deviations of mode shapes for n=0, 2, and 10 (Fig. 9f).

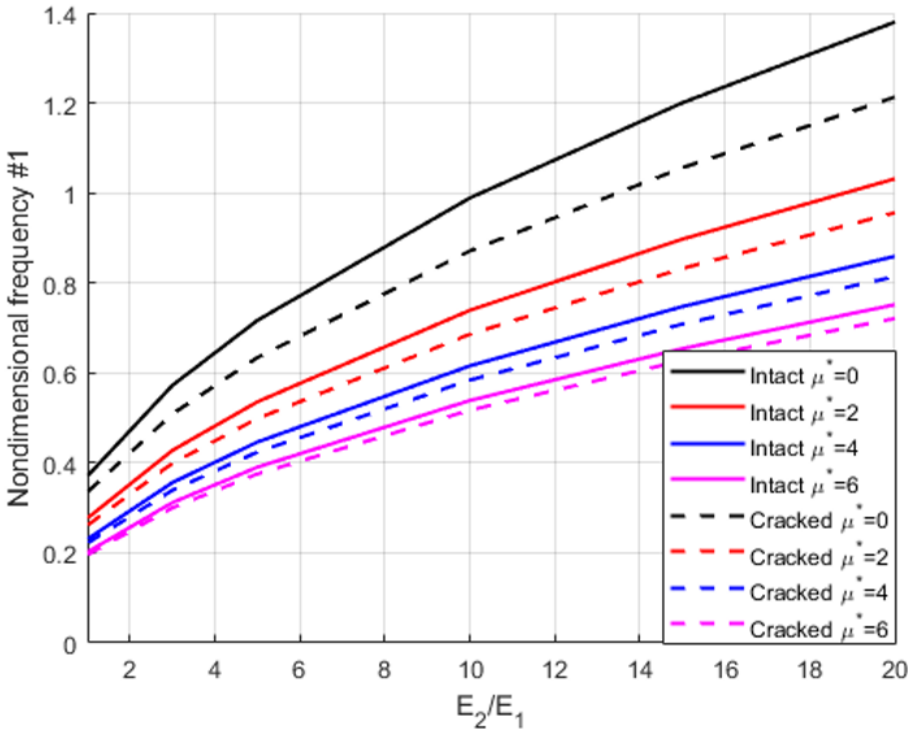

(a)

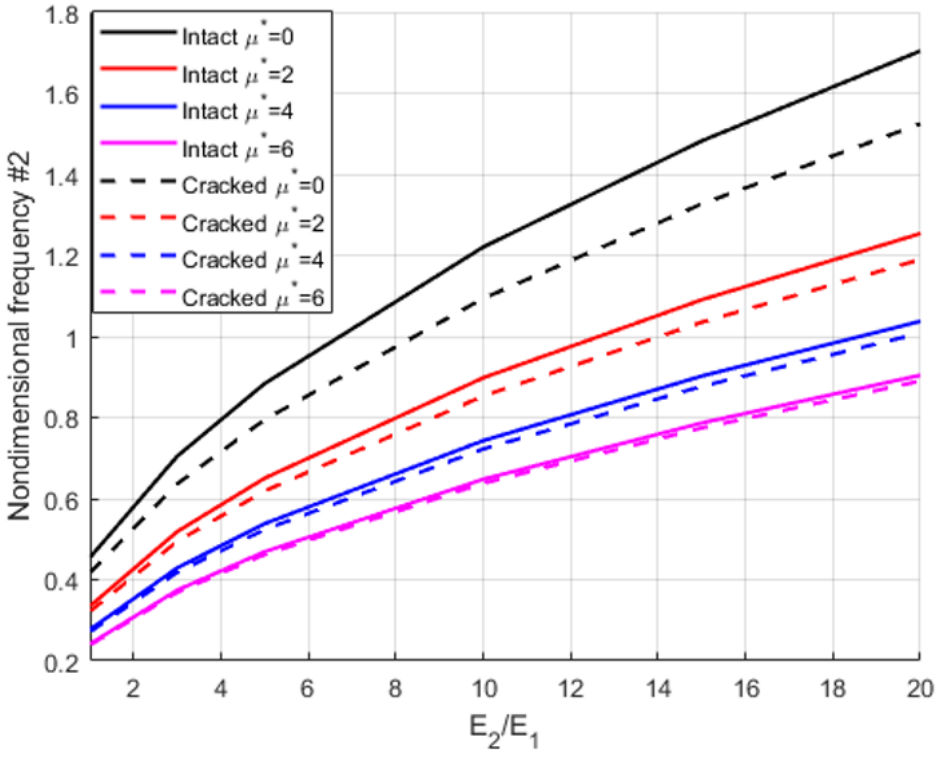

(b)

Fig. 6. Changes of the nondimensional frequencies of intact and cracked multi-span continuous FG nanobeams with nonlocal parameters and ratios of E_2/E_1: (a) 1st frequency, (b) 2rd frequency, (c) 3rd frequency.

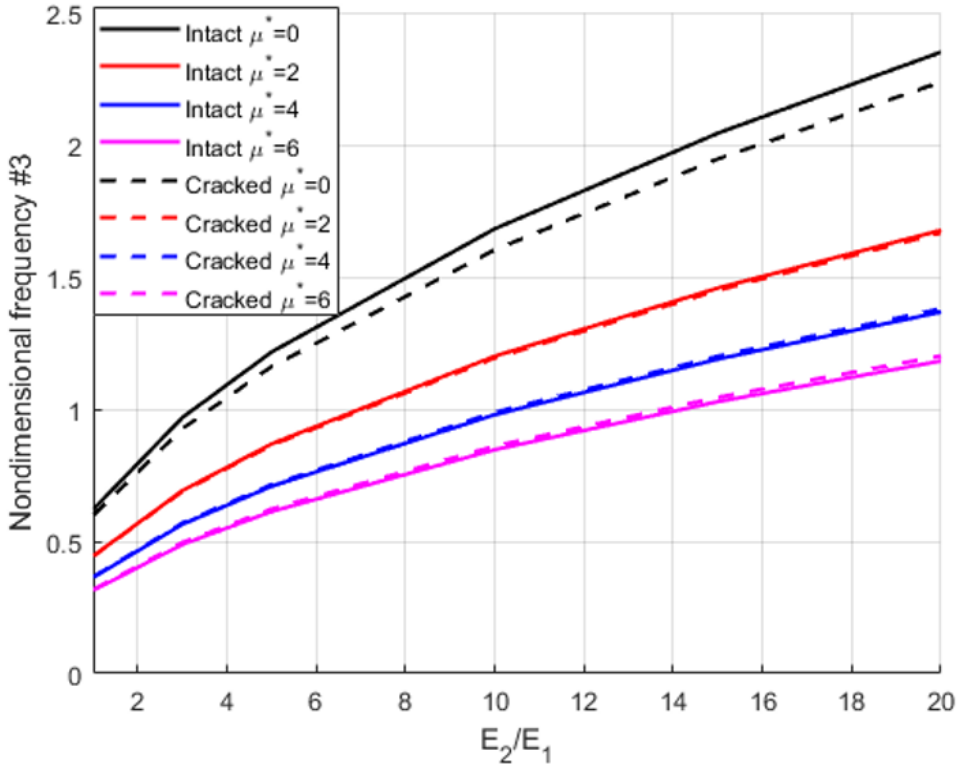

(c)

Fig. 6. (continued)

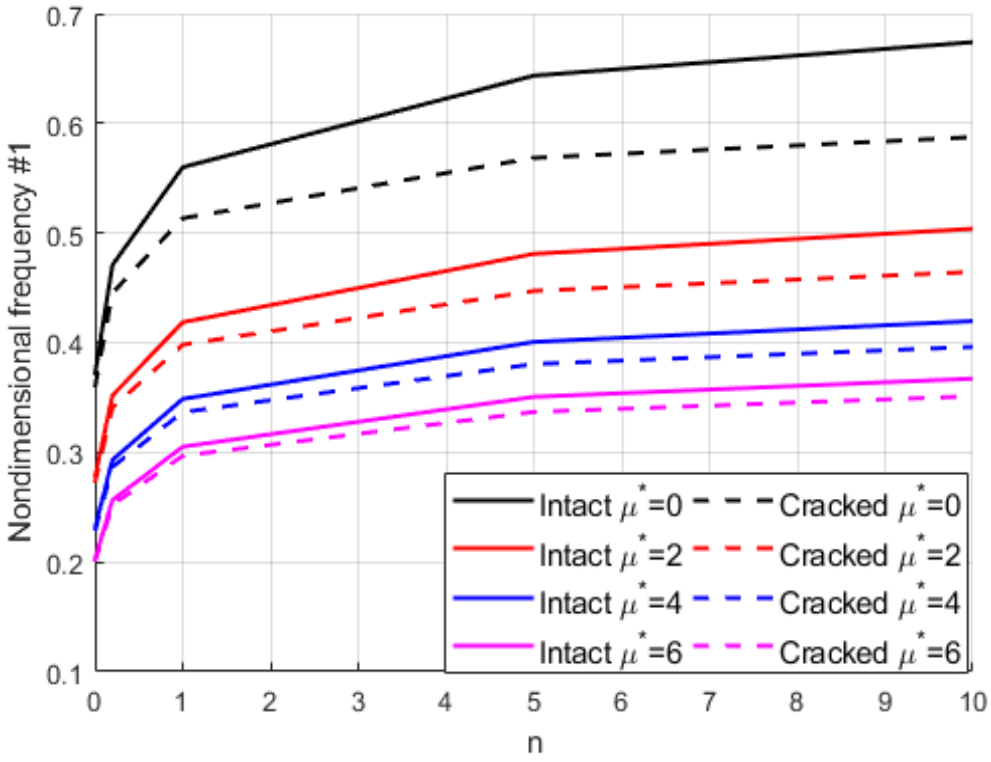

(a)

Fig. 7. Changes in the first three natural frequencies of intact and cracked multi-span continuous FG nanobeams with various nonlocal parameters and volume fraction indices: (a) 1st frequency, (b) 2nd frequency, (c) 3rd frequency

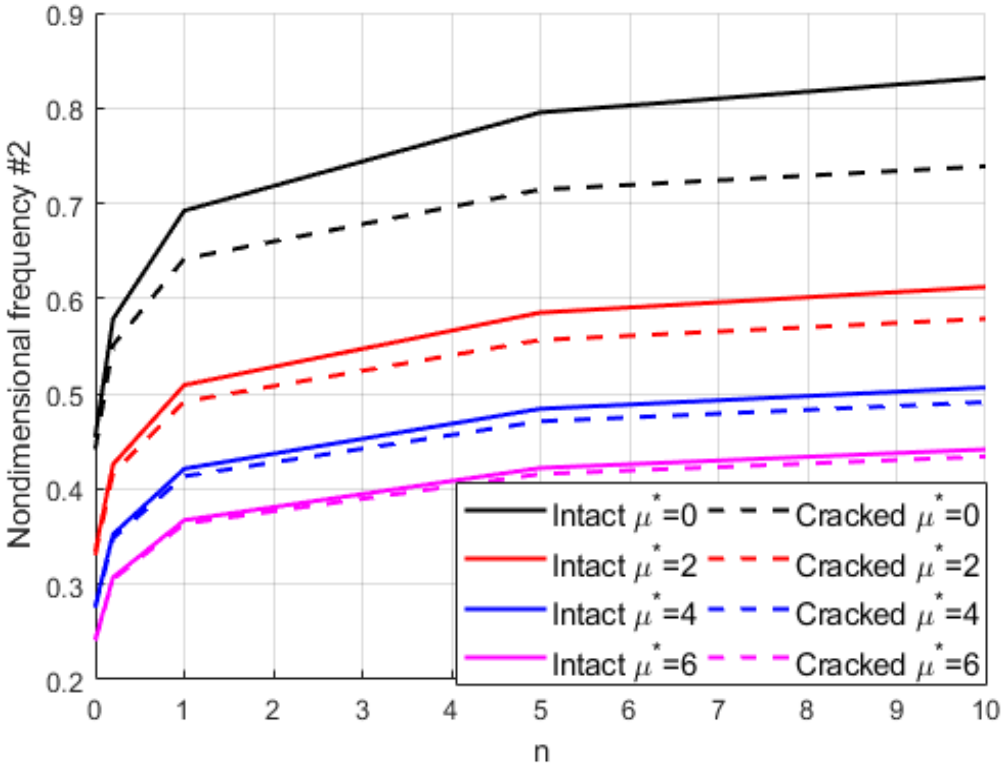

(b)

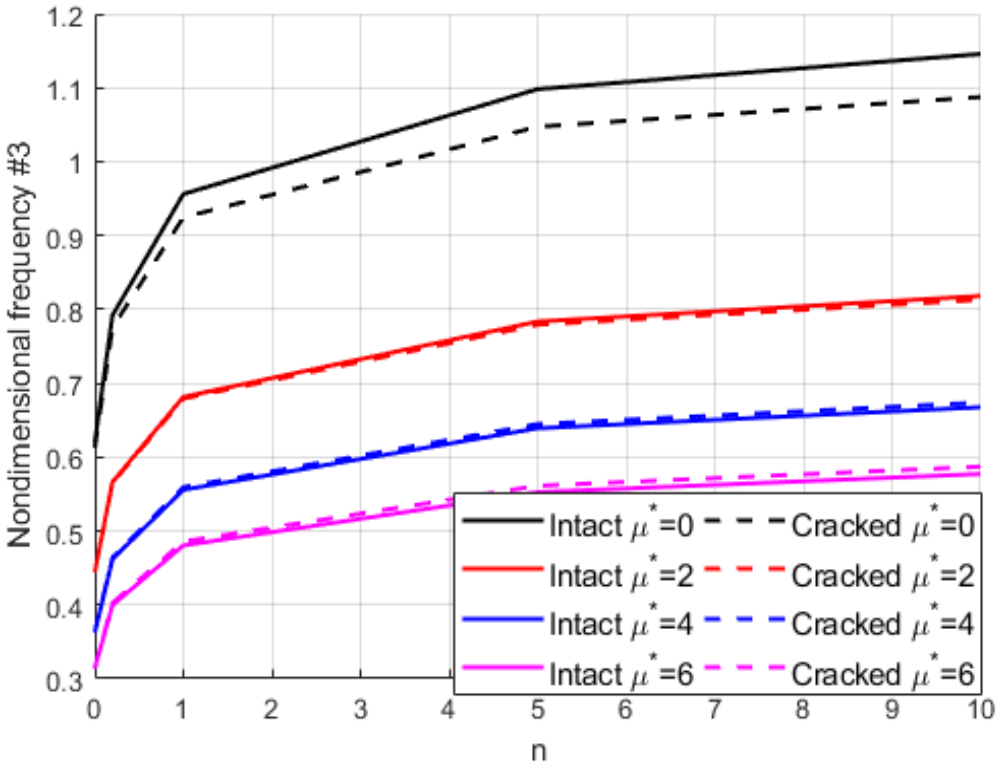

(c)

Fig. 7. (continued)

The results reveal that significant changes in the mode shapes occur only when the nonlocal parameter varies. Furthermore, the effect is considerably stronger on asymmetric mode shapes (such as the second mode) compared to symmetric ones. The mode shapes exhibit negligible changes despite differences in the associated parameters in all remaining cases. However, identifying crack

positions directly from the mode shapes remains challenging. Although discontinuities in the mode shapes can be observed at the crack locations, they are often subtle, especially when the ratio a/h is small. Analysis of mode-shape deviation plots facilitates accurate identification of crack locations. Sharp peaks are consistently observed at the crack locations, thereby suggesting that crack detection can be effectively performed using wavelet-based signal processing techniques. An increase in peak amplitude with crack depth-to-height ratio enables reliable evaluation of crack severity using wavelet coefficients.

6. Conclusions

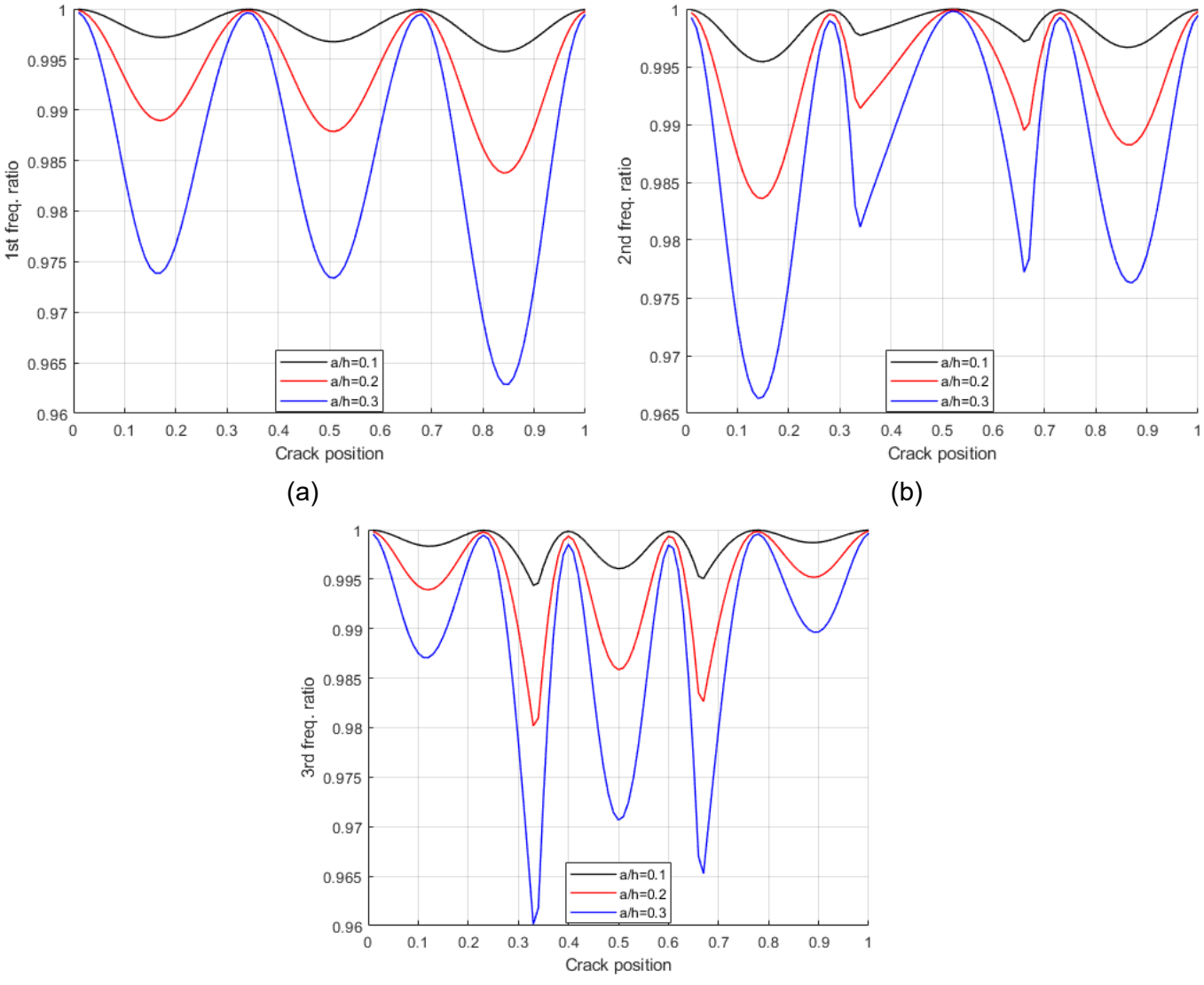

Fig. 8. Changes in the first three frequency ratios with respect to crack position varying along the nanobeam, for μ^*=2 and a/h= 0.1, 0.2, 0.3: (a) 1st frequency, (b) 2nd frequency, (c) 3rd frequency.

The main findings of this work can be summarized as follows:

A key contribution of this work is the formulation of a DSM-based model using exact vibration solutions of multiple cracked FG Euler–Bernoulli nanobeams. An important advantage of the proposed model is its ability to eliminate the nonlocal paradox in cantilever nanobeams. Furthermore, the DSM-based formulation provides an efficient and highly accurate framework for evaluating the free vibration responses of multiple cracked, multi-span continuous FG nanobeams while requiring only a very small number of elements.

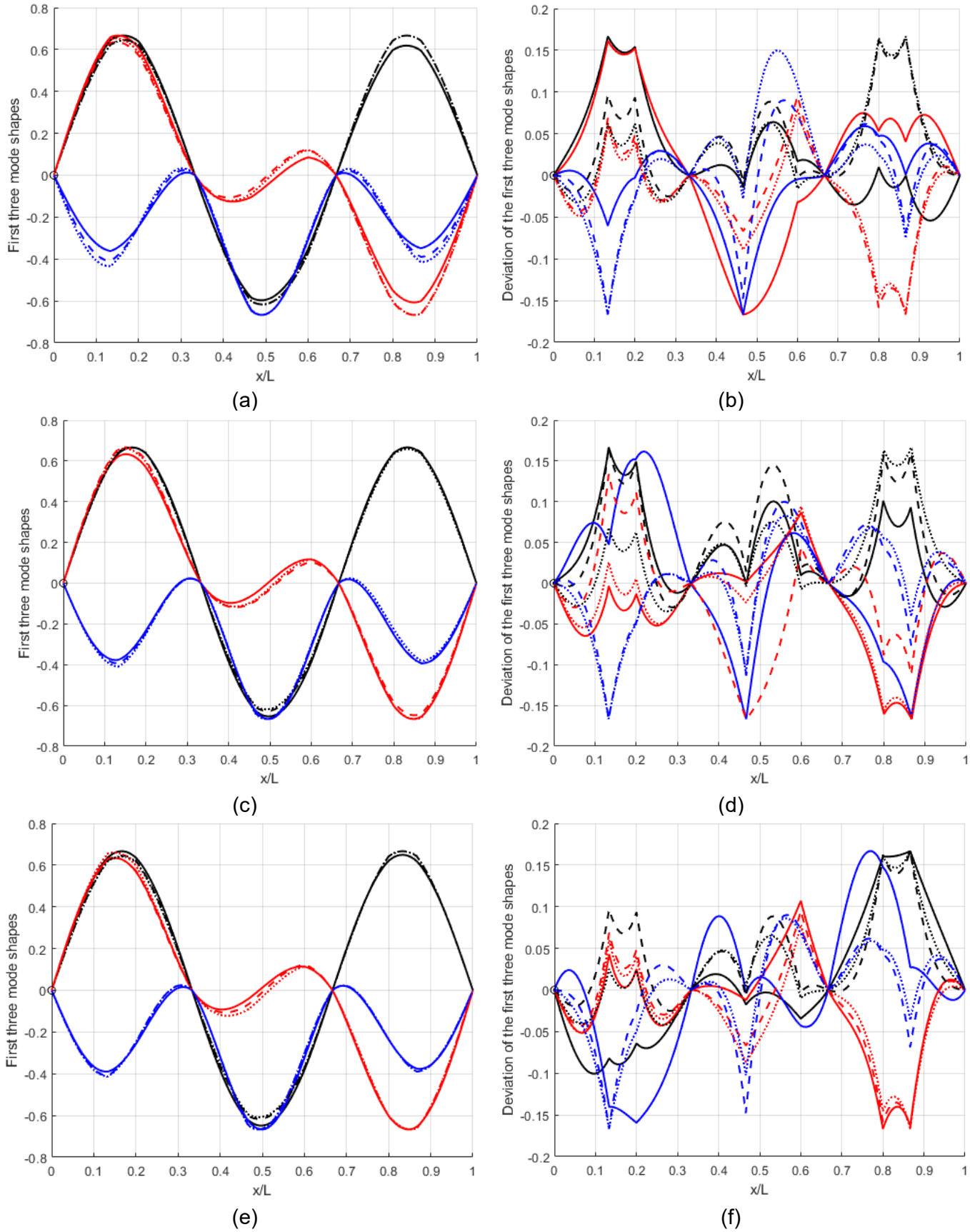

Fig. 9. The variations in the first three mode shapes of the multiple cracked multi-span continuous FG nanobeam: a) Mode shapes for nonlocal parameters: μ^*=0, 2, and 4; b) Deviations of mode shapes: μ^*=0, 2, and 4; c) Mode shapes for E_2/E_1=0.1, 2, and 10; d) Deviations of mode shapes for: E_2/E_1=0.1, 2, and 10; e) Mode shapes for: n=0, 2, and 10; f) Deviations of mode shapes for: n=0, 2, and 10.

Compared with material and crack parameters, the nonlocal parameter has a more pronounced effect, resulting in a larger decrease in the natural frequencies. This reduction is particularly pronounced in higher-order frequencies. Furthermore, the non-local parameter markedly influences the mode shapes of cracked FG nanostructures, and its impact is considerably stronger for asymmetric mode shapes. The findings clearly confirm the critical importance of non-local parameters, which must be rigorously considered in the vibration analysis of intact and cracked multi-span continuous FG nanobeams.

The presence of cracks at critical locations and increasing crack depth-to-height ratio leads to a pronounced decrease in the natural frequencies. The reduction is particularly significant for the lower order natural frequencies. In particular, the locations of the critical points, where the frequencies are least sensitive to cracks, are independent of the nonlocal parameter. The locations of critical points are consistent with those previously identified in homogeneous and FG macrobeam structures. Moreover, their positions remain unchanged regardless of the number of cracks. This observation is especially important for crack identification, since it establishes dependable reference positions where selected natural frequencies remain essentially invariant.

Direct identification of crack locations based solely on mode shapes remains difficult, especially for small crack depth-to-height ratios. Nevertheless, analysis of mode-shape deviation plots provides an effective means for detecting crack locations. Sharp localized peaks are consistently observed at crack locations in the graphs, providing a reliable basis for crack detection via wavelet transform analysis. It is also observed that deeper cracks generate higher peak amplitudes, which can be exploited as a robust metric for assessing crack depth via wavelet-based coefficients.

The results demonstrate that these effects have a significant impact on the dynamic behavior of cracked FG nanostructures. The proposed framework is readily extendable to more sophisticated cases, such as three-dimensional nanostructures under diverse boundary conditions.

Funding: This study was funded by Vietnam Ministry of Education and Training under grand number B2025.XDA.05.

Data availability: The authors declare that the data supporting the findings of this study are available within the paper.

Conflict of interests: The authors declared no potential conflicting/competing interests with respect to the research, authorship, and/or publication of this article.

Consent to participate: All authors participated in the research work reported in this paper

References

[1]. D. Karlicic, et al. (2015). Non-local Structural Mechanics. *John Wiley & Sons*. DOI: 10.1002/9781118572030

[2]. C. Polizzotto. (2001). Nonlocal elasticity and related variational principles. *International Journal of Solids and Structures*, 38(42-43), 7359-7380. DOI: 10.1016/S0020-7683(01)00039-7

[3]. M.A. Eltaher, M.E. Khater, S.A. Emam. (2016). A review on nonlocal elastic models for bending, buckling, vibrations, and wave propagation of nanoscale beams. *Applied Mathematical Modelling*, 40(5-6), 4109-4128. DOI: 10.1016/j.apm.2015.11.026

[4]. E. Ghavanloo, S.A. Fazelzadeh, F.M. de Sciarra. (2021). Size-Dependent Continuum Mechanics Approaches: Theory and Applications. Springer Cham. https://doi.org/10.1007/978-3-030-63050-8

[5]. H. Salehipour, A.R. Shahidi, H. Nahvi. (2015). Modified nonlocal elasticity theory for functionally graded materials. *International Journal of Engineering Science*, 90, 44-57. DOI: 10.1016/j.ijengsci.2015.01.005

[6]. M. Ghadiri, M. Soltanpour, A. Yazdi, M. Safi. (2016). Studying the influence of surface effects on vibration behavior of size-dependent

cracked FG Timoshenko nanobeam considering nonlocal elasticity and elastic foundation. *Applied Physics A*, 122, 520. DOI: 10.1007/s00339-016-0036-5

[7]. M. Kirkham, Z.L. Wang, R.L. Snyder. (2008). In situ growth kinetics of ZnO nanobelts. *Nanotechnology*, 19(44), 445708. DOI: 10.1088/0957-4484/19/44/445708

[8]. S.S.M.N. Souq, F.A. Ghasemi, M.M.S. Fakhrabadi. (2021). A comparative study of crack detection in nanobeams using molecular dynamics, analytical and finite element methods. *Journal of Computational Applied Mechanics*, 52(3), 408-422. DOI: 10.22059/jcamech.2021.322563.613

[9]. M. Soltanpour, M. Ghadiri, A. Yazdi, M. Safi. (2017). Free transverse vibration analysis of size dependent Timoshenko FG cracked nanobeams resting on elastic medium. *Microsystem Technologies*, 23, 1813-1830. DOI: 10.1007/s00542-016-2983-3

[10]. I. Esen, C. Özarpa, M.A. Eltaher. (2021). Free vibration of a cracked FG microbeam embedded in an elastic matrix and exposed to magnetic field in a thermal environment. *Composite Structures*, 261, 113552. DOI: 10.1016/j.compstruct.2021.113552

[11]. M.A. Attia, M.S. Matbuly, T. Osman, M. AbdElkhalek. (2024). Dynamic analysis of double cracked bi-directional functionally graded nanobeam using the differential quadrature method. *Acta Mechanica*, 235, 1961-2012. DOI: 10.1007/s00707-023-03797-8

[12]. H. Darban, R. Luciano, M. Basista. (2022). Free transverse vibrations of nanobeams with multiple cracks. *International Journal of Engineering Science*, 177, 103703. DOI: 10.1016/j.ijengsci.2022.103703

[13]. A. Hassanpour, H. Darban. (2025). Softening and Stiffening Size Effects in Free Flexural Vibration of Small-scale Cracked Beams. *Journal of Sound Vibration*, 612, 119135. DOI: 10.1016/j.jsv.2025.119135

[14]. T.V. Lien, T.B. Dinh, N.T. Thang. (2024). Exact closed-form solutions for the free vibration analysis of multiple cracked FGM nanobeams. *Proceedings of the Institution of Mechanical Engineers, Part C: Journal of Mechanical Engineering Science*, 238(8), 3373-3390. DOI: 10.1177/09544062231200608

[15]. X.-F. Li, B.-L. Wang. (2009). Vibrational modes of Timoshenko beams at small scales. *Applied Physics Letters*, 94(10), 101903. DOI: 10.1063/1.3094130

[16]. E. Ghavanloo, H. Rafii-Tabar, S.A. Fazelzadeh. (2019). Computational Continuum Mechanics of Nanoscopic Structures. *Springer*. DOI: 10.1007/978-3-030-11650-7

[17]. H. Roostai, M. Haghpanahi. (2014). Vibration of nanobeams of different boundary conditions with multiple cracks based on nonlocal elasticity theory. *Applied Mathematical Modelling*, 38(3), 1159-1169. DOI: 10.1016/j.apm.2013.08.011

[18]. A. Bahrami. (2017). A wave-based computational method for free vibration, wave power transmission and reflection in multi-cracked nanobeams. *Composites Part B: Engineering*, 120, 168-181. DOI: 10.1016/j.compositesb.2017.03.053

[19]. S. Ceballes, K. Larkin, E. Rojas, S.S. Ghaffari, A. Abdelkefi. (2021). Nonlocal elasticity and boundary condition paradoxes: a review. *Journal of Nanoparticle Research*, 23, 66. DOI: 10.1007/s11051-020-05107-y

[20]. S. Chakraverty, L. Behera. (2015). Free vibration of non-uniform nanobeams using Rayleigh–Ritz method. *Physica E: Low-dimensional Systems and Nanostructures*, 67, 38-46. DOI: 10.1016/j.physe.2014.10.039

[21]. R. Ansari, J. Torabi, A. Norouzzadeh. (2018). Bending analysis of embedded nanoplates based on the integral formulation of Eringen's nonlocal theory using the finite element method. *Physica B: Condensed Matter*, 534, 90-97. DOI: 10.1016/j.physb.2018.01.025

[22]. Nazmul I.M., Nahid S., Indronil D. (2023). Analytical solutions for vibration of Bi-directional functionally graded nonlocal nanobeams. *Results in Engineering*, 18, 101046. DOI: 10.1016/j.rineng.2023.101046

[23]. N. Challamel, Z. Zhang, C.M. Wang, J.N. Reddy, Q. Wang, T. Michelitsch, B. Collet. (2014). On nonconservativeness of Eringen's nonlocal elasticity in beam mechanics: correction from a discrete-based approach. *Archive of Applied Mechanics*, 84, 1275-1292. DOI: 10.1007/s00419-014-0862-x

[24]. P. Khodabakhshi, J.N. Reddy. (2015). A unified integro-differential nonlocal model. *International Journal of Engineering Science*, 95, 60-75. DOI: 10.1016/j.ijengsci.2015.06.006

[25]. A.I. Aria, M.I. Friswell. (2019). A nonlocal finite element model for buckling and vibration of functionally graded nanobeams. *Composites Part B: Engineering*, 166, 233-246. DOI: 10.1016/j.compositesb.2018.11.071

[26]. H.M. Numanoğlu, Ö. Civalek. (2019). On the dynamics of small-sized structures. *International Journal of Engineering Science*, 145, 103164. DOI: 10.1016/j.ijengsci.2019.103164

[27]. X.-J. Xu, Z.-C. Deng, K. Zhang, W. Xu. (2016). Observations of the softening phenomena in the nonlocal cantilever beams. *Composite Structures*, 145, 43-57. DOI: 10.1016/j.compstruct.2016.02.073

[28]. L.V. Tran, D.B. Tran, P.T. Phan. (2023). Free vibration analysis of stepped FGM nanobeams using nonlocal dynamic stiffness model. *Journal of Low Frequency Noise, Vibration and Active Control*, 42(3), 997-1017. DOI: 10.1177/14613484231160134

[29]. D.T. Hung, T.V. Lien, T.B. Dinh, N.T. Thang. (2023). Free vibration analysis of FGM framed nanostructures using variational-consistent boundary conditions. *Vietnam Journal of Mechanics*, 45(2), 164-182. DOI: 10.15625/0866-7136/18192

[30]. O.C. Zienkiewicz, R.L. Taylor, J.Z. Zhu. (2013). The finite element method: its basis and fundamentals. *Elsevier*. DOI: 10.1016/C2009-0-24909-9

[31]. E. Oñate. (2013). Structural analysis with the finite element method. Linear statics, volume 2: beams, plates and shells. Springer. DOI: 10.1007/978-1-4020-8743-1

[32]. H. Su, J.R. Banerjee. (2015). Development of dynamic stiffness method for free vibration of functionally graded Timoshenko beams. *Computers & Structures*, 147, 107-116. DOI: 10.1016/j.compstruc.2014.10.001

[33]. L.V. Tran, D.T. Ngo, K.T. Nguyen. (2019). Free and forced vibration analysis of multiple cracked FGM multi span continuous beams using dynamic stiffness method. *Latin American Journal of Solids and Structures*, 16(2), e157. DOI: 10.1590/1679-78255242

[34]. A.Y.T. Leung. (2012). Dynamic stiffness and substructures. *Springer*. DOI: 10.1007/978-1-4471-2026-1

[35]. J.R. Banerjee. (2019). Review of the dynamic stiffness method for free-vibration analysis of beams. *Transportation Safety Environment*, 1(2), 106-116. DOI: 10.1093/tse/tdz005

[36]. S. Adhikari, D. Karličić, X. Liu. (2021). Dynamic stiffness of nonlocal damped nano-beams on elastic foundation. *European Journal of Mechanics-A/Solids*, 86, 104144. DOI: 10.1016/j.euromechsol.2020.104144

[37]. M.S. Taima, T.A. El-Sayed, S.H. Farghaly. (2021). Free vibration analysis of multistepped nonlocal Bernoulli–Euler beams using dynamic stiffness matrix method. *Journal of Vibration and Control*, 27(7-8), 774-789. DOI: 10.1177/1077546320933470

[38]. T.V. Lien, et al. (2022). Free vibration analysis of FGM stepped nanostructures using nonlocal dynamic stiffness model. *Journal of Theoretical and Applied Mechanics*, 60(2), 279-292. DOI: 10.15632/jtam-pl/149175

[39]. T.B. Dinh, T.V. Lien. (2025). Free vibration analysis of multiple-cracked functionally graded

nanostructures. *Acta Mechanica*, 236, 6911-6935. DOI: 10.1007/s00707-025-04500-9

[40]. H.-S. Shen. (2016). Functionally Graded Materials: Nonlinear Analysis of Plates and Shells. *CRC Press*. DOI: 10.1201/9781420092578

[41]. M.A. Eltaher, A.A. Abdelrahman, A. Al-Nabawy, M. Khater, A. Mansour. (2014). Vibration of nonlinear graduation of nano-Timoshenko beam considering the neutral axis position. *Applied Mathematics and Computation*, 235**,** 512-529. DOI: 10.1016/j.amc.2014.03.028

[42]. A.C. Eringen. (2002). Nonlocal Continuum Field Theories. *Springer*. DOI: 10.1007/b97697

[43]. N.T. Khiem, N.N. Huyen. (2017). A method for crack identification in functionally graded Timoshenko beam. *Nondestructive Testing and Evaluation*, 32(3), 319-341. DOI: 10.1080/10589759.2016.1226304

[44]. T.G. Chondros, A.D. Dimarogonas, J. Yao. (1998). Longitudinal vibration of a continuous cracked bar. *Engineering Fracture Mechanics*, 61(5-6), 593-606. DOI: 10.1016/S0013-7944(98)00071-X

[45]. T.G. Chondros, A.D. Dimarogonas, J. Yao. (1998). A continuous cracked beam vibration theory. *Journal of Sound and Vibration*, 215(1), 17-34. DOI: 10.1006/jsvi.1998.1640

[46]. T. Yokoyama, M.-C. Chen. (1998). Vibration analysis of edge-cracked beams using a line-spring model. *Engineering Fracture Mechanics*, 59(3), 403-409. DOI: 10.1016/S0013-7944(97)80283-4

[47]. K. Aydin. (2013). Free vibration of functionally graded beams with arbitrary number of surface cracks. *European Journal of Mechanics-A/Solids*, 42, 112-124. DOI: 10.1016/j.euromechsol.2013.05.002